

Mechanical Properties and Acoustic Emission Damage Evolution of Sandy Mudstone Under Gradient Confining Pressures

Kaibo Wang

School of Energy Science and Engineering, Henan Polytechnic University, Jiaozuo, Henan 454003, China

How to cite this paper: Wang, K.B. (2026). Mechanical properties and acoustic emission damage evolution of sandy mudstone under gradient confining pressures. *Advances in Engineering Research: Possibilities and Challenges*, 4(2), 132–140. ISSN Print: 3079-5192; ISSN Online: 3079-5206.

<https://doi.org/10.63313/AERpc.9110>

Published: 2026-05-28

Copyright © 2026 by author(s) and Erytis Publishing Limited.

This work is licensed under the Creative Commons Attribution International License (CC BY 4.0).

<http://creativecommons.org/licenses/by/4.0/>



Abstract

To reveal the macroscopic deformation failure and microscopic damage evolution mechanisms of sandy mudstone under deep high in-situ stress environments, triaxial compression tests were conducted under seven gradient confining pressures (0, 2, 4, 6, 8, 10, 15 MPa), and acoustic emission (AE) signals were monitored synchronously. The effects of confining pressure on the stress-strain characteristics, strength-deformation parameters, energy evolution, macroscopic failure modes, and AE damage laws of sandy mudstone were systematically analyzed. The results show that with increasing confining pressure, the compaction stage of the stress-strain curve disappears, the plastic stage prolongs, and the post-peak attenuation slows down, presenting a transition from brittle to ductile failure. The peak strength increases linearly with confining pressure, with a cohesion of 9.44 MPa and an internal friction angle of 29.44° fitted by the Mohr-Coulomb criterion. At low confining pressure, dissipated energy mainly drives tensile crack initiation, while at high confining pressure, it dominates shear crack development. AE activity is highly coupled with stress stages, and the cumulative ringing count reaches a peak at 10 MPa. The peak damage value decreases from 0.52 at 2 MPa to 0.12 at 15 MPa, indicating that confining pressure significantly inhibits damage accumulation. This study provides an experimental and theoretical basis for stability control of deep soft rock roadways.

Keywords

Sandy Mudstone; Triaxial Compression; Confining Pressure Effect; Mechanical Properties; Acoustic Emission; Damage Evolution

1. Introduction

With the continuous increase in coal mining depth, deep roadways are often subjected to high confining pressure and complex stress environments. Sandy mudstone, as a typical soft rock and common surrounding rock in coal mines, is characterized by weak cementation, developed pores and fractures, and low strength. Under high in-situ stress, it is prone to large deformation, spalling, floor

heave, and progressive instability, which seriously restricts the safe and efficient mining of deep coal resources. The surrounding rock of deep roadways exhibits a gradient confining pressure distribution from the shallow surface to the deep interior, and the confining pressure directly dominates the mechanical response, crack propagation pattern, and damage evolution of sandy mudstone [1-2].

Extensive studies have been conducted on the mechanical properties of sandy mudstone. Zhang et al. investigated the mechanical response of sandy mudstone under post-peak cyclic loading [3], while Yu et al. analyzed the triaxial unloading characteristics after freeze-thaw cycles. Yang et al. explored the fracture mechanism under graded stress disturbance, and Chen et al. revealed the energy dissipation law [4-5]. However, most existing studies focus on single or a few confining pressure conditions, lacking systematic research on the coupling relationship between macroscopic mechanical response and microscopic damage evolution under a full gradient of confining pressures (0–15 MPa) [6-8]. In particular, the quantitative damage model based on acoustic emission and the correlation between energy distribution and failure modes are insufficiently studied [9-10].

Therefore, this paper conducts triaxial compression tests combined with real-time acoustic emission monitoring on sandy mudstone under seven gradient confining pressures. The macroscopic mechanical behavior, energy evolution, microscopic acoustic emission characteristics, and damage laws are systematically revealed, and the intrinsic mechanism of confining pressure-induced brittle-ductile transition is clarified. The research findings can provide a theoretical basis for the design and optimization of deep roadway support.

2. Test Scheme

2.1. Specimen Preparation

Homogeneous and intact sandy mudstone was collected from a deep coal mine in Henan Province. According to the International Society for Rock Mechanics (ISRM) standards, standard cylindrical specimens with a diameter of 50 mm and a height of 100 mm were processed. The end faces were ground with a double-sided grinding machine to ensure that the parallelism error of both ends was less than 0.05 mm and the vertical deviation was less than 0.25°, avoiding end effects on test results. A total of 21 qualified specimens were prepared and divided into 7 groups with 3 parallel specimens in each group, corresponding to confining pressures of 0, 2, 4, 6, 8, 10, and 15 MPa, respectively. All specimens were naturally air-dried, numbered, and recorded for size and weight to ensure test consistency.

2.2. Test Equipment

Mechanical Loading System: The RMT-15 electro-hydraulic servo rock mechanics test system was adopted, with a maximum axial load of 1000 kN and a maximum confining pressure of 60 MPa. It supports displacement/force closed-loop control

and automatically collects stress and strain data throughout the test.

Acoustic Emission Monitoring System: The DS5-8B full-information acoustic emission system was used. Two 150 kHz resonant probes were symmetrically arranged at the specimen base, with medical vaseline as the coupling agent. The threshold was set to 40 dB, and the preamplifier gain was 40 dB. The system synchronously collected ringing counts, cumulative counts, and energy signals, which were strictly time-synchronized with mechanical data.

2.3. Test Procedure

(1) **Specimen Installation:** The specimen was centered and fixed in the triaxial cell, sealed with a heat-shrinkable sleeve, and oil was injected and exhausted.

(2) **Confining Pressure Application:** The target confining pressure was applied at a constant rate and stabilized for 5 minutes.

(3) **Axial Loading:** Displacement control was adopted, with a loading rate of 0.001 mm/s for triaxial tests and 0.01 mm/s for uniaxial tests, until the specimen failed completely.

(4) **Data Synchronization:** Mechanical and acoustic emission data were collected synchronously throughout the test.

(5) **Specimen Recovery:** The macroscopic failure morphology was photographed and recorded, and the data were sorted for subsequent analysis.

3. Test Results and Analysis

3.1. Stress-Strain Curve Characteristics

The stress-strain curves of sandy mudstone under different confining pressures exhibit four typical stages: compaction, elasticity, plasticity, and post-peak failure, with confining pressure exerting a significant regulatory effect:

Compaction Stage: At low confining pressures (0–4 MPa), the curve is concave inward, corresponding to the closure of primary pores and fractures under axial load. When the confining pressure ≥ 6 MPa, the compaction stage almost disappears, as the primary defects are fully compacted by the confining pressure.

Elastic Stage: As confining pressure increases, the slope of the curve rises significantly, the elastic range expands, and the stiffness and elastic deformation capacity of the rock are enhanced.

Plastic Stage: Higher confining pressure leads to a more obvious plastic yield platform and stronger plastic deformation capacity. At low confining pressure, the plastic stage is short and yield is indistinct; at high confining pressure, the plastic stage prolongs and ductility is prominent.

Post-Peak Stage: At low confining pressure, stress drops sharply after peak, showing brittle failure; at high confining pressure, stress decreases slowly with stable residual strength, presenting ductile failure characteristics. The

stress-strain diagram of rock under different confining pressures is shown in Figure 1.

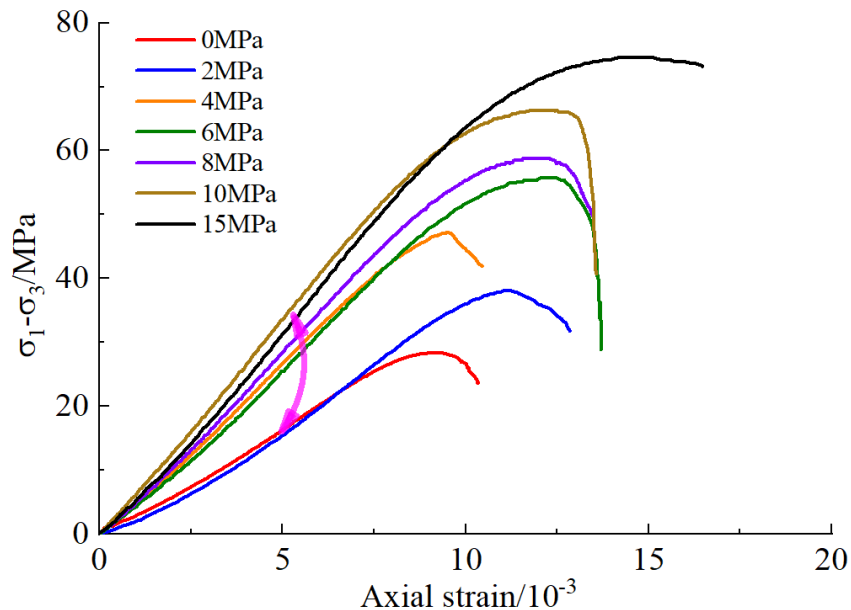


Figure 1. Stress-strain diagram of rock under different confining pressures

3.2. Strength and Deformation Parameters

The peak strength of sandy mud increases almost linearly with confining pressure. The uniaxial compressive strength is 27.45 MPa, and it rises to 87.49 MPa at 15 MPa confining pressure, with an overall increase of 218.7%. Fitted by the Mohr-Coulomb criterion, the cohesion is 9.44 MPa and the internal friction angle is 29.44°, reflecting the inherent strength properties of the rock. The strength growth rate presents a segmented feature: rapid growth at 0–4 MPa, moderate growth at 4–10 MPa, and stable growth at 10–15 MPa, which is attributed to the transition of confining pressure from compacting primary defects to inhibiting crack propagation.

The elastic modulus and deformation modulus show a consistent variation trend, rising rapidly at 0–8 MPa and then slowing down. The elastic modulus increases from 3.64 GPa at 0 MPa to 6.31 GPa at 8 MPa and 6.85 GPa at 15 MPa, while the deformation modulus rises from 3.09 GPa at 0 MPa to 5.71 GPa at 8 MPa and 6.41 GPa at 15 MPa. The peak strain is linearly positively correlated with confining pressure, with a fitting formula of $\varepsilon_1 = 9.1211 + 0.3425\sigma_3$ ($R^2 = 0.9478$). A slight decrease occurs at 2–4 MPa due to the transition from tensile to shear failure, followed by a steady increase to 14.26×10^{-3} at 15 MPa, verifying that confining pressure enhances the ductile deformation capacity of the rock. Figure 2 is a graph of the relationship between peak strain and confining pressure

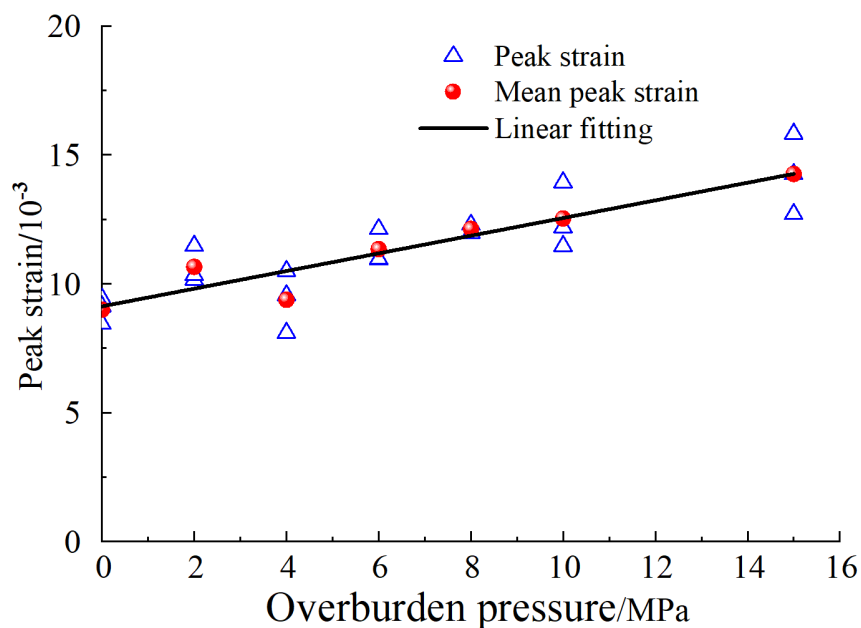


Figure 2 Stress-strain diagram of rock under different confining pressures

3.3. Energy Evolution Characteristics

Rock deformation and failure follow the law of energy conservation, where the total input energy U is converted into recoverable elastic strain energy U_e and dissipated energy U_d (including plastic deformation energy and crack propagation energy). Both pre-peak and post-peak energy increase continuously with confining pressure. The pre-peak energy rises from 0.024 kJ at 0 MPa to 0.104 kJ at 15 MPa, and the post-peak energy increases from 0.008 kJ at 0 MPa to 0.043 kJ at 15 MPa. The impact energy index (ratio of pre-peak to post-peak energy) first increases and then decreases, reaching a peak of 4.26 at 8 MPa, which is the critical threshold for the brittle-ductile transition.

At 0 MPa uniaxial compression, the proportion of elastic energy is 63.1%, plastic energy is 12.8%, and dissipated energy is 24.1%, dominated by tensile crack propagation. At 2 MPa, the proportion of plastic energy peaks at 44.2%, indicating intense plastic deformation. When confining pressure exceeds 4 MPa, the proportion of elastic energy stabilizes at around 70%, plastic energy decreases gradually, and dissipated energy increases slowly at the later stage. Low confining pressure drives tensile crack initiation, while high confining pressure inhibits tensile cracks and dominates shear crack development. The effect of confining pressure on the energy evolution characteristics of sandy mudstone is shown in Figure 3.

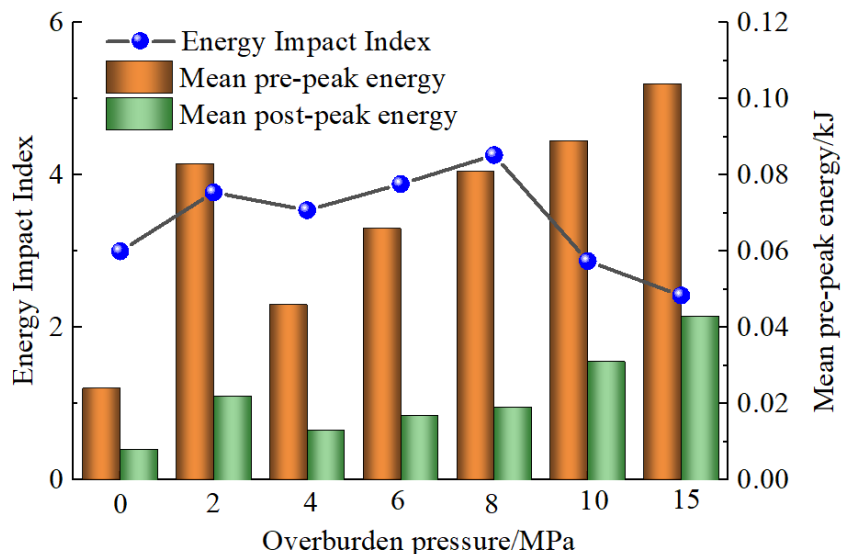
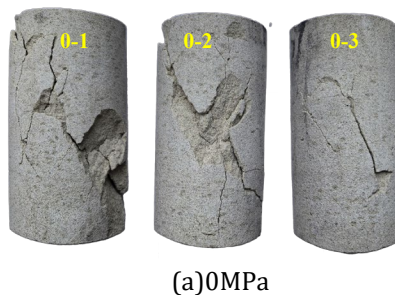


Figure 3. The Influence of Confining Pressure on the Energy Evolution Characteristics of Sandy Mudstone

3.4. Macroscopic Failure Modes

The macroscopic failure modes of sandy mudstone evolve regularly with increasing confining pressure, transitioning from brittle tensile failure to ductile shear failure. At 0 MPa uniaxial compression, the specimen shows typical brittle tensile failure with vertical through cracks and block spalling, accompanied by obvious volume expansion. At 2–4 MPa, it presents a single shear surface failure with an inclined main crack and good specimen integrity. At 6–8 MPa, it evolves into a V-shaped composite shear failure with two intersecting shear planes and developed secondary cracks. At 10–15 MPa, it exhibits a Y-shaped ductile shear failure with dense shear bands, local comminution, and prominent ductile characteristics. The macroscopic failure patterns of sandy mudstone specimens under different confining pressures are shown in Figure 4.



(a) 0MPa

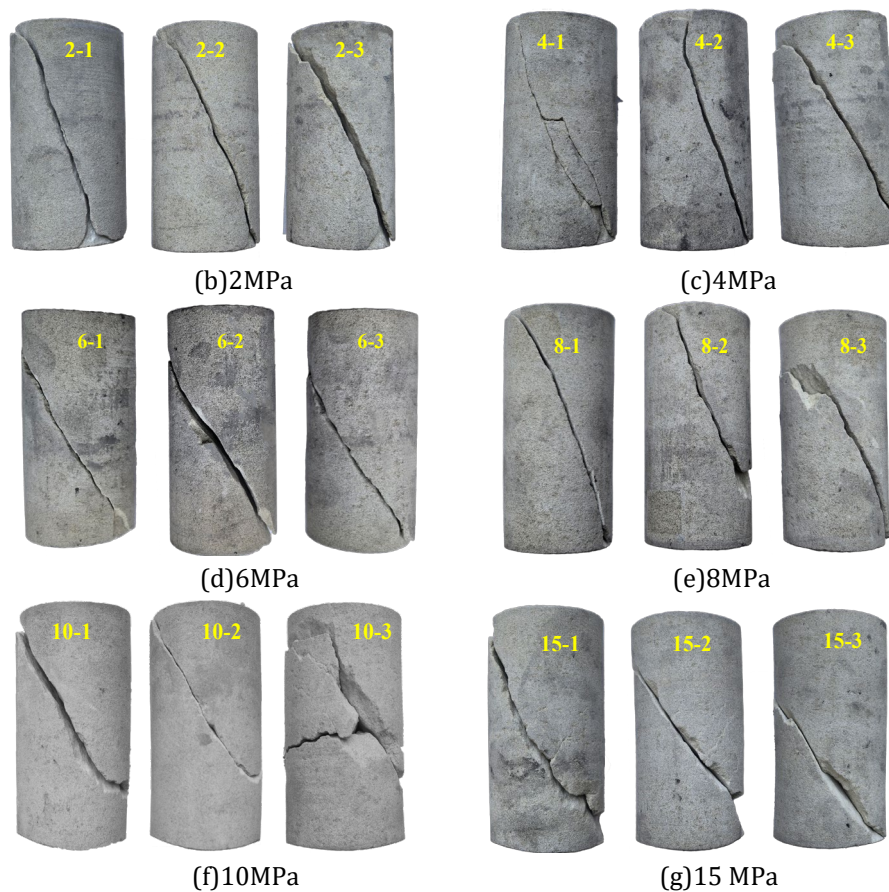


Figure 4. Macroscopic failure patterns of sandy mudstone specimens under different confining pressures

3.5. Acoustic Emission Characteristics and Damage Evolution

Acoustic emission ringing counts are highly coupled with stress stages, accurately reflecting the whole process of microcrack initiation, propagation and coalescence. In the compaction and elastic stages, ringing events are sparse with low counts, corresponding to primary crack closure and rare microcrack initiation. In the plastic stage, the ringing count rate surges with sustained activity, indicating stable propagation of new cracks. In the post-peak stage, the ringing count reaches a peak with concentrated bursts, marking the formation of macroscopic fracture surfaces through crack coalescence. Higher confining pressure delays the onset of acoustic emission activity, raising the threshold for crack initiation.

The cumulative ringing count first increases and then decreases with confining pressure, rising from 13.21×10^4 at 2 MPa to a peak of 54.15×10^4 at 10 MPa and then declining to 29.09×10^4 at 15 MPa. The 10 MPa confining pressure is the critical point for brittle-ductile transition, with the most developed microcracks. Based on Kachanov's damage theory, a damage model is established by introducing the residual strength correction, with the damage variable defined as D . Damage

evolution has three stages: initial rapid rise, stable slow rise, and explosive rise. The peak damage value decreases from 0.52 at 2 MPa to 0.12 at 15 MPa, with a decrease of 76.9%, proving that confining pressure significantly inhibits damage accumulation. The curves of damage variables versus axial strain under different confining pressures are shown in Figure 5.

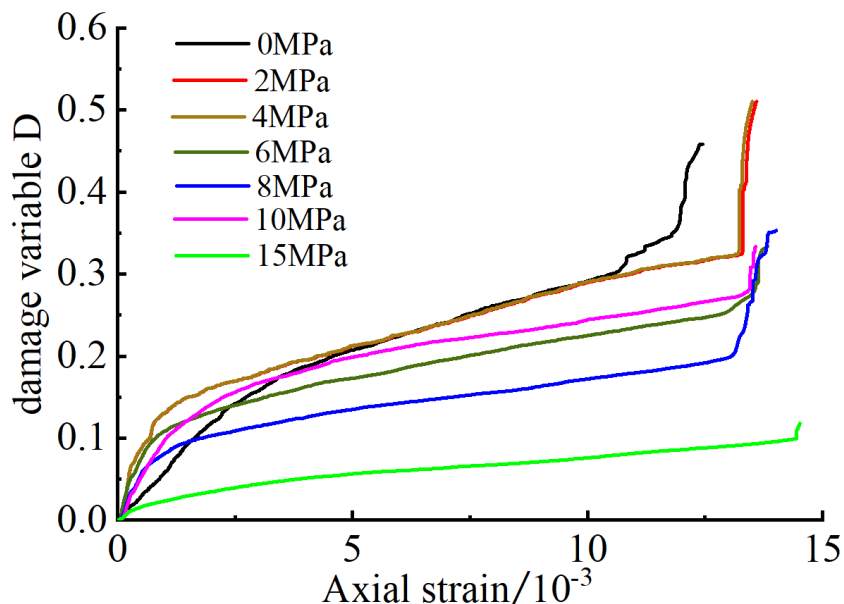


Figure 5. Damage variable-axial strain relationship curves under different confining pressures

4. Conclusions

(1) With increasing confining pressure, the stress-strain curve of sandy mudstone transitions from brittle to ductile, with the compaction stage disappearing, the plastic stage prolonging, and post-peak attenuation slowing. The peak strength increases linearly with confining pressure, with a cohesion of 9.44 MPa and an internal friction angle of 29.44°.

(2) Energy distribution is regulated by confining pressure: low confining pressure drives tensile crack initiation, while high confining pressure dominates shear crack development. The impact energy index peaks at 8 MPa, marking the brittle-ductile transition threshold.

(3) The macroscopic failure mode evolves sequentially: brittle tensile failure → single shear surface failure → V-shaped composite shear failure → Y-shaped ductile shear failure. Confining pressure inhibits tensile cracks and promotes ductile shear failure.

(4) Acoustic emission activity accurately reflects damage evolution. The cumulative ringing count peaks at 10 MPa, and confining pressure delays crack initiation and inhibits damage accumulation. The peak damage value decreases significantly with rising confining pressure.

References

- [1] Tang M Y, Gao M Z, Li S W, et al. Failure behavior and energy evolution characteristics of deep roadway sandstone under different microwave irradiation modes[J]. *Journal of Central South University*, 2023,30(1):214-226.
- [2] Li H, Xie S, Tan Y, et al. Research on the failure mechanism of anchored surrounding rock and experimental study on the control technology of anchor and pressure relief in deep gob-side entries[J]. *Engineering Failure Analysis*, 2025:110391.
- [3] Yadong C. Dynamic Response and Failure Behaviour of Tunnel Surrounding Rock with Prefabricated Cracks Under Impact Loading[J]. *Geotechnical and Geological Engineering*, 2025,44(1).
- [4] Mei W, Pan P, Wang Z, et al. Dynamic responses and failure characteristics of surrounding rock in a deep-buried tunnel with an arbitrary cross-section subjected to blasting P-wave[J]. *Computers and Geotechnics*, 2025,186:107447.
- [5] Wang Z. Research on Displacement Failure Characteristics of Deep Roadway Surrounding Rock[J]. *IOP Conference Series: Earth and Environmental Science*, 2020,565(1):12075.
- [6] Li W ,Li X ,Zhou Z , et al. Failure mode transition of layered slate under multi-level cyclic loading: from trans-layer fracture to along-layer shear slip[J].*Engineering Failure Analysis*,2026,190110717-110717.
- [7] Ma X ,Ma R ,Westman E , et al. Investigating stress evolution in rock burst prone regions in an underground mine with seismic tomographic imaging[J].*Geomechanics for Energy and the Environment*,2026,46100809-100809.
- [8] Han Y ,Jia B ,Jia J , et al. Multiscale study on the hazard evolution and risk of coal spontaneous combustion under hydrothermal action in deep mining[J].*Process Safety and Environmental Protection*,2026,210108650-108650.
- [9] Li Y ,Zhou B ,Mitri S H , et al. Evaluating the Core-Based Stress Measurement in Mining Engineering — A Critical Review of the Diametrical Core Deformation Technique[J].*Applied Sciences*,2026,16(4):2092-2092.
- [10] Zhu Y X ,Huang C Y ,Sun M .Research on a Deep Mine Cooling and Waste Heat Recovery System Driven by Large Temperature Differences between Surface and Underground[J].*Applied Geophysics*,2026,(prepublish):1-13.